forum acusticum 2026
8-12 September · Graz, Austria

A SEISMIC BARRIER STRATEGY USING AN IMPROVED RING-RESONATOR PERIODIC MATERIAL (RRPM) BASED ON 2D WFEM

Yunhe Xi[1], Mohamed Najib Ichchou[2], Imad Tawfiq[1], Olivier A. Bareille[3]

[1] *Laboratoire QUARTZ EA7393, ISAE-Supméca (Institut Supérieur de Mécanique de Paris), France*
[2] *Laboratoire de Tribologie et Dynamique des Systèmes (LTDS), ECL (École Centrale de Lyon), France*
[3] *Laboratoire de Mécanique de Normandie (LMN), INSA Rouen Normandie, France*

This paper is a revised version of the authors' submitted manuscript that was peer-reviewed by at least two anonymous reviewers.

Abstract

With the rapid expansion of urbanization, an increasing number of high-rise structures require protection from earthquake-induced damage through seismic isolation systems. However, current technologies lack effective isolation barriers capable of mitigating horizontal seismic waves. This study proposes an improved ring-resonator Unit Cell (UC) for two-dimensional (2D) periodic materials is proposed based on Bloch–Floquet theory and locally resonant mechanisms. The Wave Finite Element Method (WFEM) and Finite Element Method (FEM) are employed to investigate the Band Gap (BG) characteristics and various wave modes of the UC. Furthermore, the Transmission Loss (TL) of the proposed 2D Ring-Resonator Periodic Materials (RRPM) is validated through numerical simulations. Results demonstrate that the proposed ring-resonator UC exhibits a significantly wider and more effective band gap compared to conventional circular resonator designs.

Keywords: *Two-dimensional periodic materials, Ring-resonator, Band gap, Wave finite element method, Seismic barrier*

1. Introduction

Critical infrastructure, such as high-rise buildings, nuclear power plants, and small modular fast reactors, requires robust protection against seismic damage. To address this, periodic seismic isolation strategies have been proposed to mitigate earthquake hazards, specifically, two-dimensional (2D) periodic barriers designed to block horizontal seismic waves have gained significant attention. Moreover, recent experiments on real-size and scaled periodic materials [1], consisting of arrays of cylindrical boreholes or tubes with local resonators, have demonstrated the presence of Band Gaps (BGs) for surface waves around 50–100 Hz. These findings confirm the feasibility of utilizing such structures to protect buildings from earthquakes in real-world scenarios.

However, in conventional periodic barriers, such as the piles studied by Pu [2], the BG for surface waves (around 50 Hz) is often not sufficiently low, and the attenuation capability remains weak. Consequently, there is a distinct trend in research towards achieving lower and wider BGs with stronger attenuation. To this end, Jia [3] investigated the effects of core density and filling fraction, while Miniaci [4] proposed 3D Large-Scale Mechanical Metamaterials (LSM3). Despite these advances, traditional strategies for 2D periodic materials typically rely on increasing mass or volume, resulting in heavy and bulky solutions. In this paper, the authors propose an improved 2D Ring-Resonator Periodic Material (RRPM) characterized by a smaller scale, lighter weight, and superior attenuation performance. The proposed RRPM offers significant advantages in enhancing BG attenuation properties and conserving resources in practical engineering projects.

In this study, the Wave Finite Element Method (WFEM) and Finite Element Method (FEM) are employed to predict the BG characteristics and seismic insolation performance. The paper is organized as follows: Section 2 outlines the methodology used to calculate the dispersion curves of the Unit Cell (UC). Section 3 introduces the model and presents the results and discussion. Finally, Section 4 summarizes the conclusions and offers perspectives on future work.

2. Methodology

Infinite periodic structures can be fully characterized by a representative UC, which serves as the smallest

Corresponding author: *yunhe.xi@isae-supmeca.fr.*

non-repetitive structural component [5]. By analyzing the model of this UC, the dispersion curves for the corresponding infinite periodic structure can be derived. This section provides a brief introduction to Bloch–Floquet theory and establishes the periodic boundary conditions within the framework of the 2D WFEM [6].

2.1. Bloch-Floquet theory

Bloch–Floquet theory characterizes wave propagation in infinite periodic media, such as crystals, by relating wave functions to the reciprocal space vectors of a Bravais lattice [7]. According to this theory, the solutions to the wave equation can be expressed as:

$$\mathbf{u}(\mathbf{r}, t) = \mathrm{e}^{i(\mathbf{k}\cdot\mathbf{r}-\omega t)}\mathbf{u}_{\mathbf{k}}(\mathbf{r}) \tag{1}$$

where ω is the angular frequency, $\mathbf{u}_{\mathbf{k}}(\mathbf{r})$ is a modulation function of the displacement vector, and $\mathbf{k} = (k_x, k_y)$ denotes the wave vector in the Brillouin reciprocal space [8]. For the 2D periodic structure considered here, the periodic constant vector is $\mathbf{A} = (A_x, A_y)$. The modulation function $\mathbf{u}_{\mathbf{k}}(\mathbf{r})$ has the same periodicity as the periodic constant, which means

$$\mathbf{u}_{\mathbf{k}}(\mathbf{r}+\mathbf{A}) = \mathbf{u}_{\mathbf{k}}(\mathbf{r}) \tag{2}$$

Substituting Eq. (2) into Eq. (1) yields the following expression:

$$\begin{aligned} \mathbf{u}(\mathbf{r}+\mathbf{A}, t) &= \mathrm{e}^{\mathrm{i}(\mathbf{k}\cdot(\mathbf{r}+\mathbf{A})-\omega t)}\mathbf{u}_{\mathbf{k}}(\mathbf{r}+\mathbf{A}) \\ &= \mathrm{e}^{\mathrm{i}\mathbf{k}\cdot\mathbf{A}}\mathrm{e}^{\mathrm{i}(\mathbf{k}\cdot\mathbf{r}-\omega t)}\mathbf{u}_{\mathbf{k}}(\mathbf{r}) = \mathrm{e}^{\mathrm{i}\mathbf{k}\cdot\mathbf{A}}\mathbf{u}(\mathbf{r}, t). \end{aligned} \tag{3}$$

Eq. (3) represents the periodic boundary conditions.

2.2. 2D Wave finite element method

In the context of wave motion within infinite periodic structures, Bloch–Floquet theory governs the relationship between the displacements and forces at the boundaries of a UC. A detailed introduction to the 2D WFEM can be found in the guide provided by Cool [9]. Eq. (4) shows the equation of motion of the UC formulated directly in the frequency domain, assuming time-harmonic behaviour and neglecting damping:

$$\left(\mathbf{K} - \omega^2\mathbf{M}\right)\mathbf{q} = \mathbf{f} \tag{4}$$

where $\mathbf{K}, \mathbf{M} \in \mathbb{R}^{N\times N}$ are the stiffness and mass matrices, and $\mathbf{q}, \mathbf{f} \in \mathbb{R}^{N\times 1}$ are the nodal displacement degrees of freedom (DoFs) and the external nodal forces applied on the UC, respectively. By imposing the periodic boundary conditions derived from the Bloch–Floquet theory, the following generalized dispersion eigenvalue problem is formulated:

$$\left(\tilde{\mathbf{K}} - \omega^2\tilde{\mathbf{M}}\right)\tilde{\mathbf{q}} = \mathbf{0}, \tag{5}$$

in which $\tilde{\mathbf{K}}, \tilde{\mathbf{M}}$ are a function of k_x, k_y and given by:

$$\tilde{\mathbf{K}} = \mathbf{\Lambda_L}\mathbf{K}\mathbf{\Lambda_R}, \quad \tilde{\mathbf{M}} = \mathbf{\Lambda_L}\mathbf{M}\mathbf{\Lambda_R} \tag{6}$$

Note that $\mathbf{\Lambda_L}$ equals the conjugate transpose of $\mathbf{\Lambda_R}$. By solving this eigenvalue problem, the dispersion curves can be obtained.

3. Results and discussion

In this section, 2D UC models are first established to investigate the vibrational modes in the xy-plane, from which the dispersion curves and frequency BGs are derived using the 2D WFEM. Subsequently, the wave modes and Transmission Loss (TL) are analyzed via the FEM using COMSOL Multiphysics 6.2.

3.1. Frequency BG of the 2D RRPM

The 2D RRPM in Fig. 1a), consists of multiple local ring-resonator UCs arranged periodically along the x- and y-axes. As detailed in Fig. 1b), the UC comprises three distinct components: Part III denotes the resonator, Part II is the elastic layer, and Part I represents the matrix.

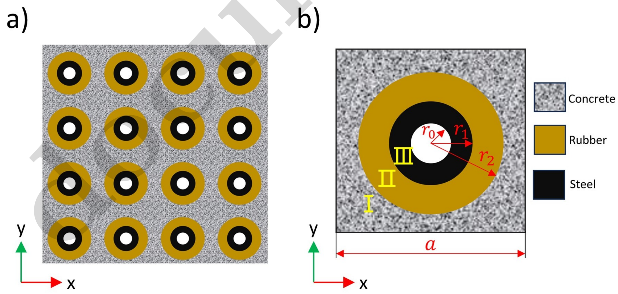

Figure 1: a) 2D RRPM b) Ring-resonator UC.

The influence of resonator geometry on the frequency BG characteristics is investigated by comparing a conventional circular resonator with the proposed improved ring-resonator. The geometric parameters for the conventional circular resonator UC are adopted from Jia. [3] as follows: $a = 1$ m, $r_2 = 0.49$ m, $r_1 = r = 0.245$ m, and $r_0 = 0$ m. To specifically evaluate the effect of the resonator shape, the resonator filling fraction is maintained constant at $\sigma = \pi r^2/a^2$. Consequently, the improved ring-resonator UC is established with the following dimensions: $a = 1$ m, $r_2 = 0.49$ m, $r_1 = 1.25r$, and $r_0 = 0.75r$. Based on these configurations, a three-component square UC is constructed using the material properties listed in Table 1.

The dispersion curves of UCs are plotted in Fig. 2, where the wave vector $\mathbf{k}$ traverses the boundaries of the first Irreducible Brillouin Zone (IBZ) along the path $\mathrm{X}-\mathrm{M}-\Gamma-\mathrm{X}$ [8]. The BGs are indicated by the yellow shaded regions. Fig. 2a) shows that the first complete BG of the circular resonator UC spans from 4.71 to 6.42 Hz. In contrast, as displayed in Fig. 2b), the first complete BG of the ring-resonator UC ranges from 4.73 to 8.22 Hz, exhibiting a significantly wider bandwidth.

Table 1: Material parameter

Material	Density ρ (kg/m^3)	Young's Modulus E (GPa)	Poisson's ratio ν
Concrete	2500	30	0.3
Rubber	1300	1.37×10^{-4}	0.463
Steel	7850	210	0.3

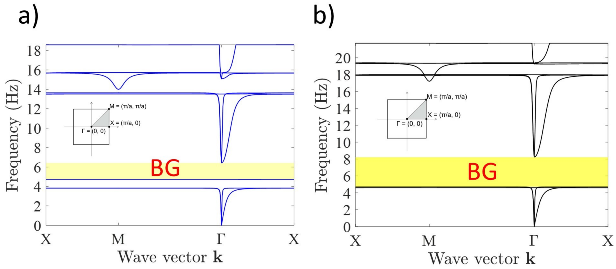

Figure 2: a) Circular resonator UC b) Ring-resonator UC.

3.2. Wave modes analysis of 2D ring-resonator UC

In this subsection, the wave modes are analyzed in detail using COMSOL Multiphysics 6.2. This analysis specifically focuses on the longitudinal wave mode propagating in the x-direction. To distinguish the longitudinal mode from other wave modes, the polarization ratio β is defined, following the method [10] as:

$$\beta = \frac{\iint_A u_x u_x^* dxdy}{\iint_A \left(u_x u_x^* + u_y u_y^*\right) dxdy} \tag{7}$$

where u_i $(i = x, y)$ denotes the components of the displacement vector, the asterisk $(*)$ represents the complex conjugate, and A signifies the entire domain of the UC. To facilitate the distinction between different wave modes, the polarization ratio β is visualized using a color map.

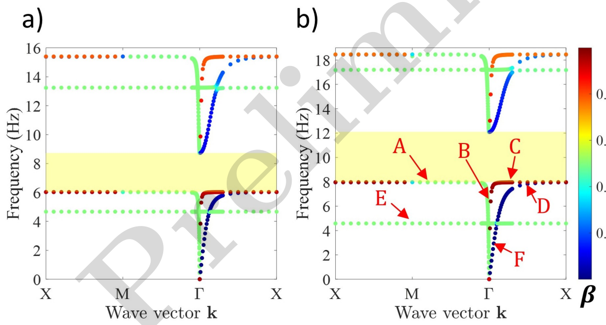

Figure 3: Dispersion curves of UCs, a) $r_1 = r$ b) $r_1 = 1.25r$, where waves modes are colored by the color map.

To compare distinct wave modes clearly, six key wave modes corresponding to points **A** through **F** are selected in Fig. 3b). Fig. 4 indicates that the modes at points **A** and **E** represent coupled modes (where the resonator vibrates in the xy-plane) within a stationary frame. Point **B** corresponds to a longitudinal mode (resonator vibrates along the x-axis) involving frame motion, whereas point **C** denotes a longitudinal mode (resonator vibrates along the x-axis) within a stationary frame. Furthermore, point **D** signifies a transversal mode (resonator vibrates along the y-axis) within a stationary frame, while point **F** exhibits a transversal mode (resonator vibrates along the y-axis) involving frame motion.

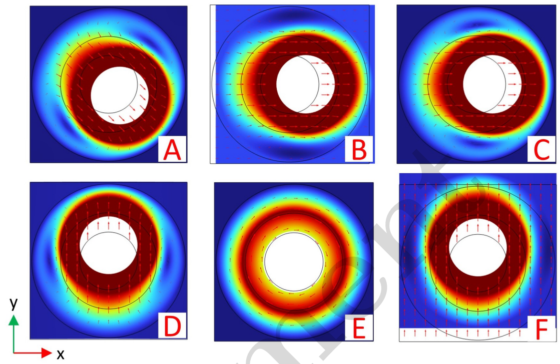

Figure 4: Displacement fields and deformation patterns for the modes marked in Fig. 3b).

3.3. Transmission loss of 2D RRPM

In Fig. 5, a finite periodic material structure composed of five ring-resonator UCs is selected for analysis. To simplify the application of boundary conditions and data extraction, additional concrete sections are appended to the structure, resulting in overall dimensions of 1 m in width and 11 m in length. The

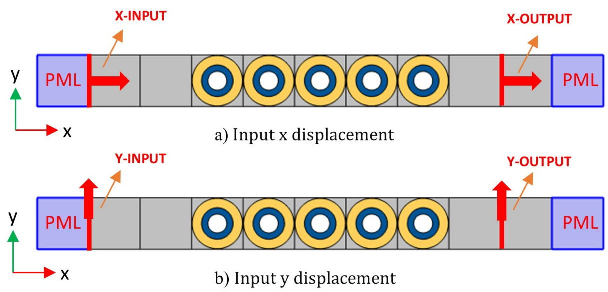

Figure 5: The xy view of RRPM.

numerical simulations focus on wave modes within the xy-plane, consequently, the thickness in the z-direction is not considered. The region on the left, labeled 'INPUT', serves as the vibration excitation zone where a uniformly distributed load is applied, while the region on the right, labeled 'OUTPUT', functions as the response measurement zone. The applied load corresponds to a displacement of 0.01 m in either the x- or y-direction. To mitigate boundary effects, Perfectly Matched Layers (PMLs) are applied to the concrete sections, and the two ends of the model are fixed.

To verify that the effective isolation frequency range of the RRPM coincides with the predicted BG, Fig. 6

presents the TL spectrum calculated using the following equation [11]:

$$T(dB) = 20\lg\frac{|U_{\text{out}}|}{|U_{\text{in}}|} \tag{8}$$

where U_{in} and U_{out} denote the average displacement amplitudes in the x- or y-direction within the left excitation ('INPUT') and right reception ('OUTPUT') zones, respectively.

In Fig. 6, the yellow shaded region indicates frequency BG of the RRPM. It is observed that the TL spectrum exhibits a sharp decline starting at the lower boundary frequency of 7.97 Hz, and the curves return to near-zero levels at the higher boundary frequency of 12.09 Hz. These results clearly demonstrate that, within the band gap, the vibration amplitude is significantly reduced. Furthermore, the TL for longitudinal waves is notably lower than that for transversal waves.

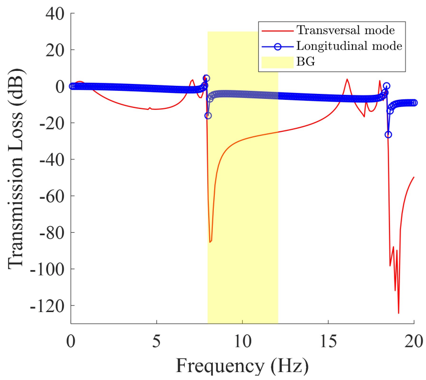

Figure 6: The TL of the RRPM.

4. Conclusion

In this paper, two approaches are employed to investigate the frequency BG and TL of the proposed RRPM. The 2D WFEM results indicate that the ring-resonator exhibits a wider low-frequency BG compared to the conventional circular resonator. Furthermore, the FEM simulations confirm that the RRPM demonstrates superior vibration attenuation performance. Considering the complex boundary conditions and diverse vibration modes inherent in building structures, seismic isolation barriers require both qualities of simplicity and flexibility, the proposed RRPM notably possesses. Consequently, the proposed 2D seismic barrier strategy using the RRPM holds significant potential for engineering applications in the seismic protection of infrastructure.

5. Acknowledgments

The authors' would like to thank China Scholarship Council (CSC) for the financial support.

References

[1] S. Brûlé, E. Javelaud, S. Enoch, and S. Guenneau, "Experiments on seismic metamaterials: Molding surface waves," *Physical review letters*, vol. 112, no. 13, p. 133 901, 2014.

[2] X. Pu and Z. Shi, "Surface-wave attenuation by periodic pile barriers in layered soils," *Construction and Building Materials*, vol. 180, pp. 177–187, 2018.

[3] G. Jia and Z. Shi, "A new seismic isolation system and its feasibility study," *Earthquake Engineering and Engineering Vibration*, vol. 9, no. 1, pp. 75–82, 2010.

[4] M. Miniaci, A. Krushynska, F. Bosia, and N. M. Pugno, "Large scale mechanical metamaterials as seismic shields," *New Journal of Physics*, vol. 18, no. 8, p. 083 041, 2016.

[5] C. Zhou, "Wave and modal approach for multi-scale analysis of periodic structures," Ph.D. dissertation, Ecole Centrale de Lyon, 2014.

[6] G. Makov and M. C. Payne, "Periodic boundary conditions in ab initio calculations," *Physical Review B*, vol. 51, no. 7, p. 4014, 1995.

[7] H. Ehrenreich, "Solid state: A new exposition: Solid state physics. neil w. ashcroft and n. david mermin. holt, rinehart and winston, new york, 1976. xxii, 826 pp., illus. 19.95.," *Science*, vol. 197, no. 4305, pp. 753–753, 1977.

[8] L. P. Bouckaert, R. Smoluchowski, and E. Wigner, "Theory of brillouin zones and symmetry properties of wave functions in crystals," *Physical Review*, vol. 50, no. 1, p. 58, 1936.

[9] V. Cool, E. Deckers, L. Van Belle, and C. Claeys, "A guide to numerical dispersion curve calculations: Explanation, interpretation and basic matlab code," *Mechanical Systems and Signal Processing*, vol. 215, p. 111 393, 2024.

[10] T.-X. Ma, Q.-S. Fan, Z.-Y. Li, C. Zhang, and Y.-S. Wang, "Flexural wave energy harvesting by multi-mode elastic metamaterial cavities," *Extreme Mechanics Letters*, vol. 41, p. 101 073, 2020.

[11] Y. Ruan, X. Liang, X. Hua, C. Zhang, H. Xia, and C. Li, "Isolating low-frequency vibration from power systems on a ship using spiral phononic crystals," *Ocean Engineering*, vol. 225, p. 108 804, 2021.